Preprint typeset in JHEP style - HYPER VERSION

Right-handed sneutrino dark matter in $\mathrm{U}(1)'$ seesaw models and its signatures at the LHC

Priyotosh Bandyopadhyay, Eung Jin Chun and Jong-Chul Park

Korea Institute for Advanced Study, Hoegiro 85, Dongdaemun-gu, Seoul 130-722, Korea
Email: priyotosh@kias.re.kr, ejchun@kias.re.kr, jcpark@kias.re.kr

Abstract: We suggest a real right-handed sneutrino, $\tilde{N}_1$, as a good dark matter candidate in a supersymmetric Z' model realizing the seesaw mechanism. When the extra gaugino, $\tilde{Z}'$, is lighter than Z', the thermal freeze-out of the dark matter annihilation to right-handed neutrinos, $\tilde{N}_1\tilde{N}_1 \to NN$, through the t-channel $\tilde{Z}'$ exchange is shown to produce the right dark matter density. It is essential to include the decay and inverse decay of N in this process, otherwise N decouples too early and thus dark matter is overproduced. At the LHC, the search for the seesaw mechanism can be made by observing the signatures of $pp \to \tilde{Z}'\tilde{Z}' \to NN + \not{p}_T$ as $\tilde{Z}'$ can be copiously produced from the cascade decays of gluinos/squarks, which is complementary to the search of $pp \to Z' \to NN$. This may also open up a promising new channel of finding the Higgs boson from the displaced N decay.

Contents

1. Introduction

Supersymmetry at the TeV scale has a nice feature that it provides a good dark matter (DM) candidate, the lightest supersymmetric particle (LSP) which is stable when R-parity is imposed for the proton stability. A typical LSP in the supersymmetric Standard Model is a neutral gaugino with a small mixture of Higgsinos whose relic density is naturally in the right range due to its weak interaction property [1]. The supersymmetric Standard Model may be extended to include a new sector in which the LSP resides. The observed neutrino masses and mixing require such an extension in various ways [2]. A standard example is to introduce right-handed neutrinos which are singlets of the Standard Model (SM) gauge group and have only Yukawa interactions with active neutrinos. Then, a right-handed sneutrino, which is the scalar superpartner of a right-handed neutrino, can be the LSP and thus a dark matter candidate. However, the cosmic production mechanism of the right-handed sneutrino dark matter can be different from the usual neutralino.

If neutrinos are Dirac particles without invoking the seesaw mechanism, the required neutrino Yukawa coupling is of order 10^{-13}, and thus the right-handed sneutrino can never

be thermalized. However, thermal regeneration through the tiny Dirac neutrino Yukawa coupling can be effective to produce a sizable abundance of the right-handed sneutrino [3]. If the seesaw mechanism is realized at the TeV scale, one has the neutrino Yukawa coupling of order 10^{-7} which, then, leads to the overproduction of the right-handed sneutrino LSP. To avoid this, there must be a thermalization process through which its relic density can be suppressed appropriately. One of the earliest proposals for such a thermalization is to assume an unconventionally large A term leading to a sizable mixing between the left-handed and right-handed sneutrinos [4]. More recently, the non-minimal supersymmetric Standard Model was considered to allow a coupling of the right-handed neutrino with an extra singlet field introduced in the Higgs sector [5]. Note also that one can invoke the inverse seesaw mechanism which allows for a possibility of order-one neutrino Yukawa couplings [6].

In this paper, we propose a new way of generating thermal freeze-out density of the right-handed sneutrino dark matter in $U(1)'$ seesaw models which may arise from a grand unification group [7]. In the case of Dirac neutrino models with no lepton number violation, the right thermal abundance was shown to be generated through the Z' resonance enhancement of the right-handed sneutrino annihilation [8]. However, this feature is not shared with $U(1)'$ models realizing the seesaw mechanism in which (complex) right-handed sneutrino components are split into two real scalar fields, an LSP and a heavier state, with a large mass difference driven by the lepton number violating soft (Majorana) mass term and they couple non-diagonally to the Z' gauge boson. Thus, the Z' interaction is typically too weak to prevent the overproduction of the right-handed sneutrino LSP.

It will be shown that the right-handed sneutrino annihilation to right-handed neutrinos through the t-channel $U(1)'$ gaugino, $\tilde{Z}'$, exchange can be efficient enough to produce the observed dark matter density. In this process, the decays and inverse decays of the right-handed neutrinos through the small Yukawa coupling play an important role in keeping the right-handed neutrinos in thermal equilibrium and thus controlling the dark matter relic density, which is a distinguishable feature of the thermal history of the right-handed sneutrino dark matter compared with the conventional neutralino LSP dark matter. From the numerical analysis of the Boltzmann equations, we will show how the dark matter freeze-out density arises depending particularly on the $\tilde{Z}'$ mass and the effective neutrino mass corresponding to the dark matter sneutrino Yukawa coupling.

Searching for an extra gauge boson Z' through dilepton resonances is one of the key issues in collider experiments [9]. A novel feature of $U(1)'$ seesaw models is that right-handed neutrinos can be produced directly from the Z' decay and their subsequent decay leaves a clean signature of same-sign dileptons appearing at sizable displaced vertices depending on the corresponding neutrino mass [10, 11]. Observing these signals at the LHC will indicate the Majorana nature of neutrinos confirming the seesaw mechanism [12]. Furthermore, it provides an interesting possibility to discover the Higgs boson through displaced b-jets [13] coming from the right-handed neutrino decay. The supersymmetric model with the right-handed sneutrino LSP enjoys these features with the production of $\tilde{Z}'$ and its decay to the right-handed neutrino and sneutrino dark matter. Independently of the Z' production, $\tilde{Z}'$ can be produced copiously from the cascade decays of gluinos and squarks, and

thus the search for the presence of the Majorana right-handed neutrino can be made more effectively. In particular, it is expected to have a large number of events for the same-sign dilepton or four displaced b-jets plus large missing energy from pair-produced $\tilde{Z}'$ if it is the next LSP.

This paper is organized as follows. In Section 2, we introduce a $U(1)'$ seesaw model, and analyze the masses of Z' and $\tilde{Z}'$ and interaction vertices relevant for our calculation. In Section 3, the thermal abundance of right-handed sneutrino dark matter is calculated for various model parameters such as the masses of $\tilde{Z}'$ and the right-handed (s)neutrino, the neutrino Yukawa coupling, and the $U(1)'$ gauge coupling. In Section 4, LHC signatures of the model are discussed focusing on the pair production of the right-handed neutrinos from the decay of Z' and $\tilde{Z}'$, which can provide a test for the seesaw mechanism and a new channel for the Higgs production. We conclude in Section 5.

2. A supersymmetric U(1)′ seesaw model

Among various possibilities of an extra gauge symmetry $U(1)'$ and the presence of the associated right-handed neutrinos [7], we will take the $U(1)_\chi$ model for our explicit analysis. The particle content of our $U(1)_\chi$ model is as follows:

$SU(5)$	10_F	$\bar{5}_F$	$1(N)$	5_H	$\bar{5}_H$	$1(X)$	$1(S_1)$	$1(S_2)$
$2\sqrt{10}Q'$	-1	3	-5	2	-2	0	10	-10

(2.1)

where $SU(5)$ representations and $U(1)'$ charges of the SM fermions $(10_F, \bar{5}_F)$, Higgs bosons $(5_H, \bar{5}_H)$, and additional singlet fields $(N, S, S'_{1,2})$ are shown. Here N denotes the right-handed neutrino, X is an additional singlet field fit into the 27 representation of E_6, and we introduced more singlets $S_{1,2}$, vector-like under $U(1)'$, to break $U(1)'$ and generate the Majorana mass term of N. Note that the right-handed neutrinos carry the largest charge under $U(1)_\chi$ and thus the corresponding Z' decays dominantly to right-handed neutrinos. Furthermore, the additional singlet field X is neutral under $U(1)_\chi$ so that it can be used to generate a mass to the $U(1)'$ Higgsinos as will be discussed below. The gauge invariant superpotential in the seesaw sector is given by

$$W_{seesaw} = y_{ij} L_i H_u N_j + \frac{\lambda_{N_i}}{2} S_1 N_i N_i \,, \tag{2.2}$$

where L_i and H_u denote the lepton and Higgs doublet superfields, respectively. After the $U(1)'$ breaking by the vacuum expectation value $\langle S_1 \rangle$, the right-handed neutrinos obtain the mass $m_{N_i} = \lambda_{N_i} \langle S_1 \rangle$ and induce the seesaw mass for the light neutrinos:

$$\widetilde{m}^\nu_{ij} = -y_{ik} y_{jk} \frac{\langle H_u^0 \rangle^2}{m_{N_k}} \,. \tag{2.3}$$

To generate the atmospheric neutrino mass $\widetilde{m}_\nu = 0.05$ eV with the right-handed neutrino mass scale of $m_N \sim 100$ GeV, we need the Yukawa coupling of $y_\nu \sim 4 \times 10^{-7}$. For the breaking of $U(1)'$, one can consider the following schemes. The first option is to introduce the μ' term [14]:

$$W' = \mu' S_1 S_2 \,, \tag{2.4}$$

and arrange radiative $U(1)'$ breaking with a large Yukawa coupling, say λ_{N_3}, mimicking the electroweak breaking in the Minimal Supersymmetric Standard Model (MSSM). Another possibility is to consider

$$W' = \lambda X S_1 S_2 + \frac{\kappa}{3} X^3 \tag{2.5}$$

as in the non-minimal Higgs sector [15]. The corresponding scalar potential is given by

$$V = V_{\rm susy} + V_{\rm soft} + V_D \ , \tag{2.6}$$

where

$$V_{\rm susy} = \sum_{\phi=X,S_1,S_2,N_i,H_u,L_i} \left| \frac{\partial W}{\partial \phi} \right|^2 \ , \tag{2.7}$$

$$\begin{aligned} V_{\rm soft} = & \left[y_\nu A_\nu \tilde{L} H_u \tilde{N} + \frac{\lambda_N}{2} A_N S_1 \tilde{N} \tilde{N} + \lambda A_S X S_1 S_2 + \frac{\kappa}{3} A_\kappa X^3 + h.c. \right] \\ & + m_X^2 |X|^2 + m_S^2 \left[|S_1|^2 + |S_2|^2 \right] + m_{\widetilde{N}}^2 |\widetilde{N}|^2 \ , \end{aligned} \tag{2.8}$$

$$V_D = \frac{g'^2}{2} \left[Q'_{S_1} |S_1|^2 + Q'_{S_2} |S_2|^2 + Q'_N |\widetilde{N}|^2 + \cdots \right]^2 \ . \tag{2.9}$$

In this case, the μ' term is generated through the vacuum expectation value of X: $\mu' = \lambda \langle X \rangle$ which, in the leading term, is given by

$$\mu' \sim \frac{\lambda}{4\kappa} \left(A_\kappa + \sqrt{A_\kappa^2 - 8 m_S^2} \right) \ , \tag{2.10}$$

where A_κ is the trilinear soft term and m_S is the soft mass of S [15]. The vacuum expectation values of $S_{1,2}$ can be developed radiatively for $\lambda \sim 1$.

Given the vacuum expectation values $\langle S_{1,2} \rangle$, one gets the Z' gauge boson mass: $M_{Z'}^2 = 2 g'^2 \sum_i Q'^2_{S_i} \langle S_i \rangle^2$ where g' denotes the $U(1)'$ gauge coupling. At the moment, the most stringent bound on the Z' mass comes from the electroweak precision data. For the $U(1)_\chi$ model, we get $M_{Z'} > 1.14$ TeV for the reference gauge coupling $g' = \sqrt{5/3} g_2 \tan\theta_W \approx 0.46$ [16], which gives $\langle S_i \rangle > 800\,\text{GeV}$ for $\langle S_1 \rangle = \langle S_2 \rangle$. Note that the value of the gauge coupling g' can be scaled down depending on the particle content below the grand unification scale. For our numerical analysis, we will take the above reference value.

Important mass parameters for our analysis are the $U(1)'$ gaugino mass and the dark matter mass. Defining $\tan\beta' = \langle S_2 \rangle / \langle S_1 \rangle$, the $U(1)'$ gaugino-Higgsino mass matrix in the basis of $[\tilde{Z}', \tilde{S}_1, \tilde{S}_2]$ is given by

$$\mathcal{M} = \begin{bmatrix} m_M & M_{Z'} c_{\beta'} & -M_{Z'} s_{\beta'} \\ M_{Z'} c_{\beta'} & 0 & \mu' \\ -M_{Z'} s_{\beta'} & \mu' & 0 \end{bmatrix} \ , \tag{2.11}$$

where m_M is the soft supersymmetry breaking mass. In the limit of $\mu' \gg m_M, M_{Z'}$, the lightest state has the mass $m_{\tilde{Z}'}$ given by $m_{\tilde{Z}'} \approx m_M + M_{Z'}^2 s_{2\beta'} / \mu'$. In the following, we will work in this limit. As a light $\tilde{Z}'$ is favored for our dark matter relic density, we will work in this limit taking $m_{\tilde{Z}'}$ as a free parameter without bothering the specific values of

$\tan\beta'$ and μ'. Among three right-handed neutrino superfields, let us take the lightest one N (we will suppress the flavor index in the following discussions) whose scalar component contains the LSP. Denoting its supersymmetric mass by m_N, the right-handed sneutrino $\tilde{N}$ has the mass terms:

$$V_{mass} = (m_N^2 + m_{\tilde{N}}^2 - \frac{1}{4}M_{Z'}^2 c_{2\beta'})|\tilde{N}|^2 - \frac{1}{2}B_N m_N(\tilde{N}\tilde{N} + \tilde{N}^*\tilde{N}^*) \,, \tag{2.12}$$

where $B_N m_N = -\lambda_N A_N \langle S_1\rangle$. Due to the lepton number violating (Majorana) mass term of $B_N m_N$ which is assumed to be positive, the real and imaginary components of the sneutrino, $\tilde{N} = (\tilde{N}_1 + i\tilde{N}_2)/\sqrt{2}$, get a mass splitting and their masses are given by $m_{\tilde{m}_{1,2}}^2 = m_N^2 + m_{\tilde{N}}^2 - \frac{1}{4}M_{Z'}^2 \mp B_N m_N$. The real scalar field $\tilde{N}_1$ is taken to be the LSP dark matter.

2.1 Couplings of N and $\tilde{N}_1$ with Higgses

From the superpotential in Eq. (2.2), simplified here as $W_{seesaw} = y_\nu L H_u N + \frac{1}{2}m_N NN$, and the soft terms in Eq. (2.8), one can find the couplings of N and $\tilde{N}$ involving leptons/sleptons and the Higgs bosons. For this, one uses the usual transformation to the Higgs mass eigenstates as follows:

$$\begin{aligned}
H_d^0 &= \frac{1}{\sqrt{2}}\left(v_d + h_d^0 + i a_d^0\right) \,, \quad H_u^0 = \frac{1}{\sqrt{2}}\left(v_u + h_u^0 + i a_u^0\right) \,, \\
h_d^0 &= \cos\alpha\, H - \sin\alpha\, h \,, \quad h_u^0 = \sin\alpha\, H + \cos\alpha\, h \,, \\
a_d^0 &= \sin\beta\, A - \cos\beta\, G^0 \,, \quad a_u^0 = \cos\beta\, A + \sin\beta\, G^0 \,, \\
H_d^\pm &= \sin\beta\, H^\pm - \cos\beta\, G^\pm \,, \quad H_u^\pm = \cos\beta\, H^\pm + \sin\beta\, G^\pm \,,
\end{aligned} \tag{2.13}$$

where $\tan\beta = v_u/v_d$ and $\tan 2\alpha = \tan 2\beta(\frac{m_A^2 + M_Z^2}{m_A^2 - M_Z^2})$.

Then the right-handed neutrino N has the coupling with the left-handed neutrino ν and charged lepton l:

$$\mathcal{L}_{NL} = \frac{y_\nu}{\sqrt{2}} N\nu\,(h\cos\alpha + H\sin\alpha + iA\cos\beta) - y_\nu\, N l H^+ \cos\beta + h.c. \tag{2.14}$$

in the Weyl fermion notation. Due to the vacuum expectation values of the Higgs bosons, there arises mixing between N and ν and the corresponding mixing angle is given by

$$\theta_{N\nu} \approx \frac{y_\nu v_u}{\sqrt{2}m_N} \,. \tag{2.15}$$

This mixing induces the N–ν–Z and N–l–W^+ interaction leading to the N decay to the usual gauge bosons. For completeness, let us write down the scalar interaction of $\tilde{N} = (\tilde{N}_1 + i\tilde{N}_2)/\sqrt{2}$:

$$\begin{aligned}
V_{\tilde{N}\tilde{L}} = {} & y_\nu m_N \tilde{\nu} H_u^0 \tilde{N}^* + y_\nu \tilde{\nu}(A_L H_u^0 - \mu H_d^{0*})\tilde{N} \\
& - y_\nu m_N \tilde{l} H_u^+ \tilde{N}^* - y_\nu \tilde{l}(A_L H_u^+ + \mu H_d^+)\tilde{N} + h.c. \,,
\end{aligned} \tag{2.16}$$

from which one can read off the couplings in terms of the mass eigenstates. The above scalar interaction leads also to mixing between $\tilde{N}$ and $\tilde{\nu}$ whose mixing angle is given by

$$\theta_{\tilde{N}_{1,2}\tilde{\nu}_{R,I}} = y_\nu \frac{(m_N \pm A_L \mp \mu\cot\beta)v_u}{\sqrt{2}(m_{\tilde{N}_{1,2}}^2 - m_{\tilde{\nu}_{R,I}}^2)} \,. \tag{2.17}$$

2.2 Decay of the right-handed neutrino N

From the couplings (2.14) and the mixing (2.15), various channels open up as the decay modes of the right-handed neutrino, N. The corresponding decay widths are given as follows:

$$\Gamma(N \to \nu h) = \Gamma\left(N \to \bar{\nu} h\right) = \frac{1}{8}\frac{y_\nu^2 m_N}{8\pi}\left(1 - \frac{m_h^2}{m_N^2}\right)^2 \cos^2\alpha \,, \tag{2.18}$$

$$\Gamma(N \to \nu H) = \Gamma\left(N \to \bar{\nu} H\right) = \frac{1}{8}\frac{y_\nu^2 m_N}{8\pi}\left(1 - \frac{m_H^2}{m_N^2}\right)^2 \sin^2\alpha \,,$$

$$\Gamma(N \to \nu A) = \Gamma\left(N \to \bar{\nu} A\right) = \frac{1}{8}\frac{y_\nu^2 m_N}{8\pi}\left(1 - \frac{m_A^2}{m_N^2}\right)^2 \cos^2\beta \,,$$

$$\Gamma(N \to l H^+) = \Gamma(N \to \bar{l} H^-) = \frac{1}{4}\frac{y_\nu^2 m_N}{8\pi}\left(1 - \frac{m_{H^\pm}^2}{m_N^2}\right)^2 \cos^2\beta \,,$$

$$\Gamma(N \to \nu Z) = \Gamma(N \to \bar{\nu} Z) = \frac{1}{8}\frac{y_\nu^2 m_N}{8\pi}\left(1 - \frac{M_Z^2}{m_N^2}\right)^2 \left(1 + 2\frac{M_Z^2}{m_N^2}\right) \sin^2\beta \,,$$

$$\Gamma(N \to l W^+) = \Gamma(N \to \bar{l} W^-) = \frac{1}{8}\frac{y_\nu^2 m_N}{8\pi}\left(1 - \frac{M_W^2}{m_N^2}\right)^2 \left(1 + 2\frac{M_W^2}{m_N^2}\right) \sin^2\beta \,.$$

To quantify these decays, we will use the notion of the effective neutrino mass defined by

$$\tilde{m}_\nu \equiv \frac{y_\nu^2 v_u^2}{2 m_N} \tag{2.19}$$

which can be of order of the observed neutrino mass or smaller.

2.3 Couplings of Z' and $\tilde{Z}'$

The $U(1)'$ gauge boson and gaugino couplings in our model is summarized in Table 1. For the Higgs–neutralino(chargino)–$\tilde{Z}'$ coupling, the diagonalization matrices of the usual neutralinos and charginos are defined by

$$\begin{aligned} \tilde{H}_u^0 &= N_{4i}\lambda_i^0 \,, \quad \tilde{H}_d^0 = N_{3i}\lambda_i^0 \\ \tilde{H}_u^+ &= V_{2i}\lambda_i^+ \,, \quad \tilde{H}_d^- = U_{2i}\lambda_i^- \end{aligned} \tag{2.20}$$

in the two component notation. Moreover, the four component mass eigenstates are defined in terms of the two component fields as

$$\chi_i^0 = \begin{pmatrix} \lambda_i^0 \\ \overline{\lambda}_i^0 \end{pmatrix} \,, \quad \chi_i^+ = \begin{pmatrix} \lambda_i^+ \\ \overline{\lambda}_i^- \end{pmatrix} \,. \tag{2.21}$$

3. Relic density of the right-handed sneutrino dark matter

In this section, we will calculate the thermal relic abundance of the right-handed sneutrino DM $\widetilde{N}_1$. Since the DM particle $\widetilde{N}_1$ cannot annihilate through the Z' interaction, one may

$\bar{f}fZ'$	$ig'(Q'_{f_L}P_L - Q'_{f_R^\dagger}P_R)\gamma^\mu$	hAZ'	$-ig'Q'_{H_u}\sin(\alpha+\beta)q^\mu$
$\tilde{f}\tilde{f}^*Z'$	$ig'Q'_f q^\mu$	HAZ'	$ig'Q'_{H_u}\cos(\alpha+\beta)q^\mu$
$\tilde{f}_L\bar{f}\tilde{Z}'$	$-i\sqrt{2}g'Q'_{f_L}P_R$	H^+H^-Z'	$ig'Q'_{H_u}q^\mu$
$\tilde{f}_R\bar{f}\tilde{Z}'$	$-i\sqrt{2}g'Q'_{f_R^\dagger}P_L$	hZZ'	$-i\sqrt{2}g'M_Z Q'_{H_u}\cos(\alpha+\beta)g^{\mu\nu}$
$\tilde{N}_1\tilde{N}_2Z'$	$ig'Q'_N q^\mu$	HZZ'	$-i\sqrt{2}g'M_Z Q'_{H_u}\sin(\alpha+\beta)g^{\mu\nu}$
$\bar{N}\tilde{N}_1\tilde{Z}'$	$-ig'Q'_N P_R$	$h\bar{\chi}_i^0\tilde{Z}'$	$-ig'Q'_{H_u}(N_{4i}\cos\alpha + N_{3i}\sin\alpha)P_R$
$\bar{N}\tilde{N}_2\tilde{Z}'$	$g'Q'_N P_R$	$H\bar{\chi}_i^0\tilde{Z}'$	$-ig'Q'_{H_u}(N_{4i}\sin\alpha - N_{3i}\cos\alpha)P_R$
$S_{1,2}S^*_{1,2}Z'$	$ig'Q'_{S_{1,2}}q^\mu$	$A\bar{\chi}_i^0\tilde{Z}'$	$g'Q'_{H_u}(N_{4i}\cos\beta - N_{3i}\sin\beta)P_R$
$\bar{\tilde{S}}_{1,2}\tilde{S}_{1,2}Z'$	$ig'Q'_{S_{1,2}}\gamma^\mu$	$H^+\bar{\chi}_i^+\tilde{Z}'$	$-i\sqrt{2}g'Q'_{H_u}(V^*_{2i}\cos\beta\, P_R - U_{2i}\sin\beta\, P_L)$
$S_{1,2}\bar{\tilde{S}}_{1,2}\tilde{Z}'$	$-i\sqrt{2}g'Q'_{S_{1,2}}P_R$		

Table 1: Couplings of Z' and $\tilde{Z}'$ in the $U(1)_\chi$ model where g' and Q_X are the $U(1)_\chi$ gauge coupling and charge of the field X, respectively, and q^μ denotes the 4-momentum difference between two bosons in the vertex.

consider its annihilation to right-handed neutrinos through the t-channel $\widetilde{Z}'$ exchange. In this case, the question is whether the right-handed neutrino N remains sufficiently in thermal equilibrium. Consequently, it is very crucial to study the interaction rate for reactions of N. As will be shown in detail, the Z' interaction of N alone is too weak to give the right dark matter relic density but the inclusion of the decay and inverse decay of N can significantly change the result. For the following analyses, we will assume the numerical values of $m_h = 115$ GeV, $\tan\beta = 10$, and $g' = 0.46$ unless otherwise stated.

3.1 Freeze out of $\widetilde{N}_1$

The annihilation cross section of the DM candidate $\tilde{N}_1$ through the process, $\tilde{N}_1\tilde{N}_1 \to NN$, can be large enough to suppress arbitrarily its relic density depending on mass parameters such as $m_{\widetilde{N}_1}, m_N$, and $m_{\widetilde{Z}'}$ as far as N is in thermal equilibrium long enough. However, the interaction of N is either through the heavy gauge boson Z' or the tiny neutrino Yukawa coupling y_ν and thus might be too weak to keep N in thermal equilibrium during the process of freeze-out of $\tilde{N}_1$. Thus, to study the thermal history of $\widetilde{N}_1$ through the annihilation in Figure 1(a), one has to consider also the evolution of N determined by its annihilation (Figure 1 (b)) and decay (Figure 1 (c), (d)).

For the analysis of the relic abundance of the $\widetilde{N}_1$, let us set up the following coupled Boltzmann equations for the evolution of the number density n_i of particle i:

$$\frac{dn_{\widetilde{N}_1}}{dt} = -3Hn_{\widetilde{N}_1} - \langle\sigma_{\widetilde{N}_1}v_{\widetilde{N}_1}\rangle\left[(n_{\widetilde{N}_1})^2 - \left(\frac{g_{\widetilde{N}_1}}{g_N}n_N\right)^2\right], \tag{3.1}$$

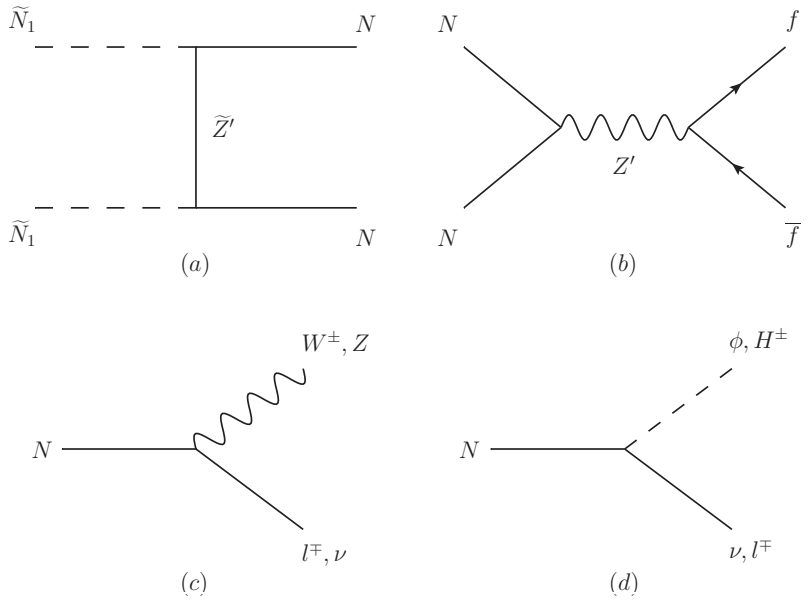

Figure 1: Annihilation and decay channels of $\widetilde{N}_1$ and N. In panel (d), $\phi = h, H$ and A.

$$\frac{dn_N}{dt} = -3Hn_N - \langle\sigma_N v_N\rangle\left[(n_N)^2 - (n_N^{\rm eq})^2\right] + \langle\sigma_{\widetilde{N}_1} v_{\widetilde{N}_1}\rangle\left[(n_{\widetilde{N}_1})^2 - \left(\frac{g_{\widetilde{N}_1}}{g_N} n_N\right)^2\right] - \Gamma_N(n_N - n_N^{\rm eq}) \,, \tag{3.2}$$

where H is the Hubble parameter, and $n_i^{\rm eq}$, v_i and g_i are respectively the equilibrium number density, relative velocity and number of internal degrees of freedom of particle i. The first terms on the right-hand sides of Eqs. (3.1) and (3.2) account for the dilution due to the expansion of the Universe. The second term on the right-hand side of Eq. (3.1) describes the forward and backward reactions of $\widetilde{N}_1\widetilde{N}_1$ annihilation to NN through the t-channel $\widetilde{Z}'$ exchange (Figure 1 (a)). The second term on the right-hand side of Eq. (3.2) refers to the forward and backward reactions of NN annihilation to the SM fermion pairs $f\overline{f}$ through the s-channel Z' exchange (Figure 1 (b)). The third term represents the effects of $\widetilde{N}_1\widetilde{N}_1$ annihilation to NN through the t-channel $\widetilde{Z}'$ exchange (Figure 1 (a)). The last term describes the decays and inverse decays of the right-handed neutrinos shown in Figure 1 (c), (d).

In solving the Boltzmann equations (3.1) and (3.2), it is useful to introduce the variable $Y_i \equiv n_i/s$ describing the actual number of particle i per comoving volume, where s is the entropy density of the Universe. Solving the coupled differential equations (3.1) and (3.2), one can find Y_i as a function of $x \equiv m_{\widetilde{N}_1}/T$.

In order to see the effect of the decay more clearly, let us first present the solutions of the coupled Boltzmann equations excluding the last term on the right-hand side of Eq. (3.2) which accounts for the decays and inverse decays of the right-handed neutrino. The result is shown in Figure 2, where we use the following mass parameters: $m_{\widetilde{N}_1} = 300$ GeV, $m_N = 260$ GeV, $m_{\widetilde{Z}'} = 600$ GeV, and $M_{Z'} = 1200$ GeV. Since $\widetilde{N}_1$ can remain in

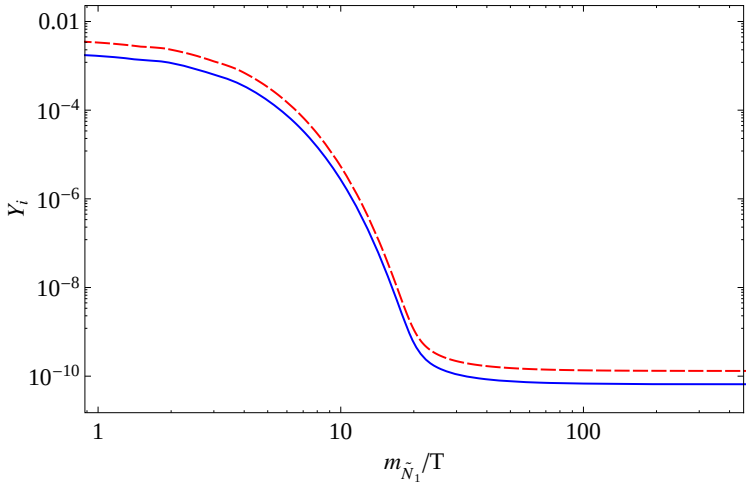

Figure 2: The actual number of $\widetilde{N}_1$ and N per comoving volume without the decay effect term. Blue solid and red dashed lines show $Y_{\widetilde{N}_1} \equiv n_{\widetilde{N}_1}/s$ and $Y_N \equiv n_N/s$ respectively. The other parameters are fixed as follows: $m_{\widetilde{N}_1} = 300$ GeV, $m_N = 260$ GeV, $m_{\widetilde{Z}'} = 600$ GeV, and $M_{Z'} = 1200$ GeV.

thermal bath through the interactions of N, the freeze out temperature of $\widetilde{N}_1$ is determined by that of N, if the interactions of N are weaker than those of $\widetilde{N}_1$. Therefore, without the decay effect term, $\widetilde{N}_1$ is decoupled from thermal equilibrium when N is decoupled as can be seen from Figure 2.

The right-handed neutrino mostly annihilates to SM fermion-antifermion pairs $f\overline{f}$ through the s-channel Z' exchange, but the cross section for this process $NN \to f\overline{f}$ is suppressed by large Z' gauge boson mass, $M_{Z'} > 1.14$ TeV [16]. Moreover, in the zero-velocity limit, this annihilation cross section of right-handed neutrinos is more suppressed since the annihilation cross section for this process has no s-wave component. Thus, the annihilation of the right-handed neutrino usually freezes out earlier than that of the right-handed sneutrino DM candidate. Consequently, the right-handed sneutrino $\widetilde{N}_1$ is generically overproduced due to the early decoupling of N as shown in Figure 3.

The decays and inverse decays of right-handed neutrinos through the Yukawa coupling y_ν turn out to play a crucial role in evading the previous overproduction problem. In Figure 4, we present the evolution of the number density of $\widetilde{N}_1$ and N per comoving volume for four representative values $\widetilde{m}_\nu = 10^{-2}, 10^{-3}, 10^{-5}$, and 10^{-6} eV. In this analysis, we use the same values for the other parameters as in the analysis of Figure 2. For larger values of light neutrino mass ($\widetilde{m}_\nu \gtrsim 10^{-3}$ eV), *i.e.* larger Yukawa coupling y_ν, the N decay term of Eq. (3.2) is strong enough to dominate other interaction terms of N before the annihilation effect of N becomes weaker than the dilution effect due to the expansion of the Universe. Therefore, the decay effect keeps N in thermal equilibrium for a longer time compared with the case that N is stable, and N can continuously remain in thermal bath before $\widetilde{N}_1$ is decoupled from thermal bath as can be seen from the top two panels of Figure 4. On the other hand, for smaller light neutrino masses ($\widetilde{m}_\nu \lesssim 10^{-3}$ eV), the

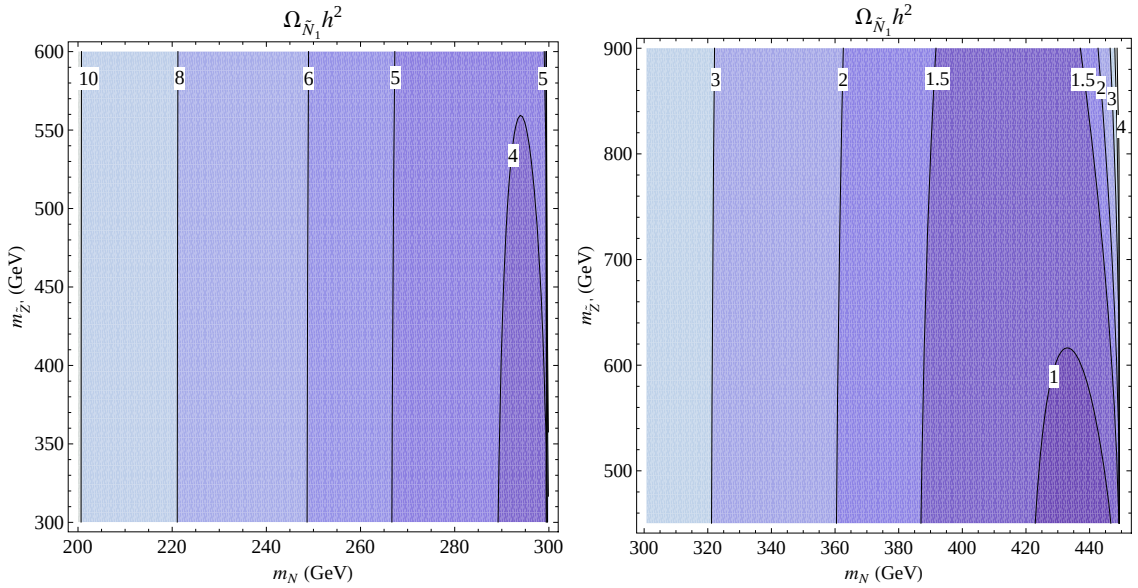

Figure 3: Contour plots for the relic abundance of the right-handed sneutrino dark matter $\widetilde{N}_1$ in the $m_N - m_{\widetilde{Z}'}$ plane when the decay effect of N is excluded. Each panel shows the cases $m_{\widetilde{N}_1} =$ 300 and 450 GeV, respectively. We fix the Z' gauge boson mass as $M_{Z'} = 1200$ GeV.

annihilation effect of N becomes weaker than the dilution effect before the N decay effect dominates other reactions. As a result, a retarded behavior appears in the number density evolution of $\widetilde{N}_1$ and N as can be seen from the bottom two panels of Figure 4. In addition, since the decay modes of N are governed by the Dirac neutrino Yukawa coupling y_ν, *i.e.* the effective neutrino mass $\widetilde{m}_\nu$, the result in Figure 4 converges to the one in Figure 2 for smaller $\tilde{m}_\nu$.

3.2 Dependence on $m_{\widetilde{N}_1}$

In this and the following subsections, we will obtain the thermal relic abundance of right-handed sneutrino $\Omega_{\widetilde{N}_1}h^2$ given mass parameters including $m_{\widetilde{N}_1}, m_N, \widetilde{m}_\nu, m_{\widetilde{Z}'}$, $M_{Z'}$ and also the $U(1)'$ gauge coupling g' by solving the coupled Boltzmann equations (3.1) and (3.2) including the decay term. In order to see the dependence of the relic abundance on each parameter, we search for the allowed regions, which satisfy the observed recent DM relic density limit [17], in the m_N–$m_{\widetilde{Z}'}$ plane fixing the other parameters.

In Figure 5, the m_N–$m_{\widetilde{Z}'}$ parameter space is explored for the six cases of the right-handed sneutrino dark matter mass: $m_{\widetilde{N}_1} = 150$, 300, 450, 600, 750 and 900 GeV. Our numerical analysis is performed in the case of $M_{Z'} = 1200$ GeV and $\widetilde{m}_\nu = 10^{-3}$ eV. The region between two thick dashed lines represents points where $\Omega_{\widetilde{N}_1}h^2$ is consistent with the recent WMAP result on the DM relic density [17]. As one can see in Figure 5, the right-handed sneutrino mass less than 900 GeV, $m_{\widetilde{N}_1} < 900$ GeV, is allowed by the recent WMAP result.

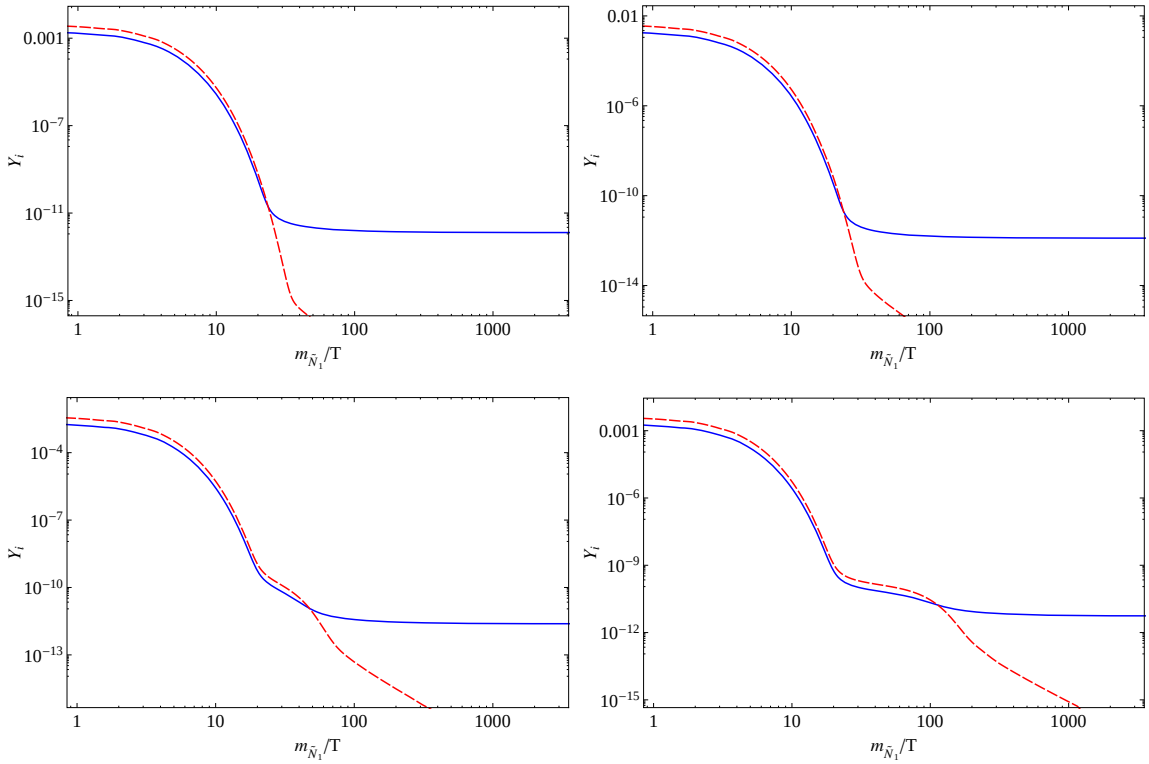

Figure 4: The actual number of $\widetilde{N}_1$ and N per comoving volume. The panels correspond to $\widetilde{m}_\nu = 10^{-2}, 10^{-3}, 10^{-5}$ and 10^{-6} eV respectively from left to right and top to bottom. Blue solid and red dashed lines show $Y_{\widetilde{N}_1} \equiv n_{\widetilde{N}_1}/s$ and $Y_N \equiv n_N/s$. The other parameters are the same as in the analysis of Figure 2.

3.3 Dependence on $\widetilde{m}_\nu$

The right-handed sneutrino DM particle $\widetilde{N}_1$ can remain in thermal equilibrium through the interactions of the right-handed neutrino N for which the inclusion of the decay effect is crucial as shown already. In this subsection, we study this effect in more detail by changing the neutrino Yukawa coupling y_ν, that is, the effective neutrino mass $\tilde{m}_\nu$. In Figure 6, the thermal relic density $\Omega_{\widetilde{N}_1} h^2$ is shown for the two representative cases $\widetilde{m}_\nu = 10^{-1}$ and 10^{-5} eV in the m_N–$m_{\widetilde{Z}'}$ plane to be compared with Figure 5. We use the numerical values $m_{\widetilde{N}_1} = 300$ GeV and $M_{Z'} = 1200$ GeV for this analysis.

For smaller effective neutrino mass, the decay rate of the right-handed neutrino is weaker, and consequently the right-handed sneutrino DM particle is decoupled earlier from thermal equilibrium. As a result, the relic abundance $\Omega_{\widetilde{N}_1} h^2$ increases as $\widetilde{m}_\nu$ decreases. This implies that smaller $\tilde{Z}'$ mass is required for smaller $\tilde{m}_\nu$. One can see the tendency from the top-middle panel of Figure 5 and Figure 6.

3.4 Dependence on $M_{Z'}$

The right-handed sneutrino DM $\widetilde{N}_1$ is kept in thermal equilibrium through the interactions of the right-handed neutrino N which also depends on the Z' mass as the right-handed

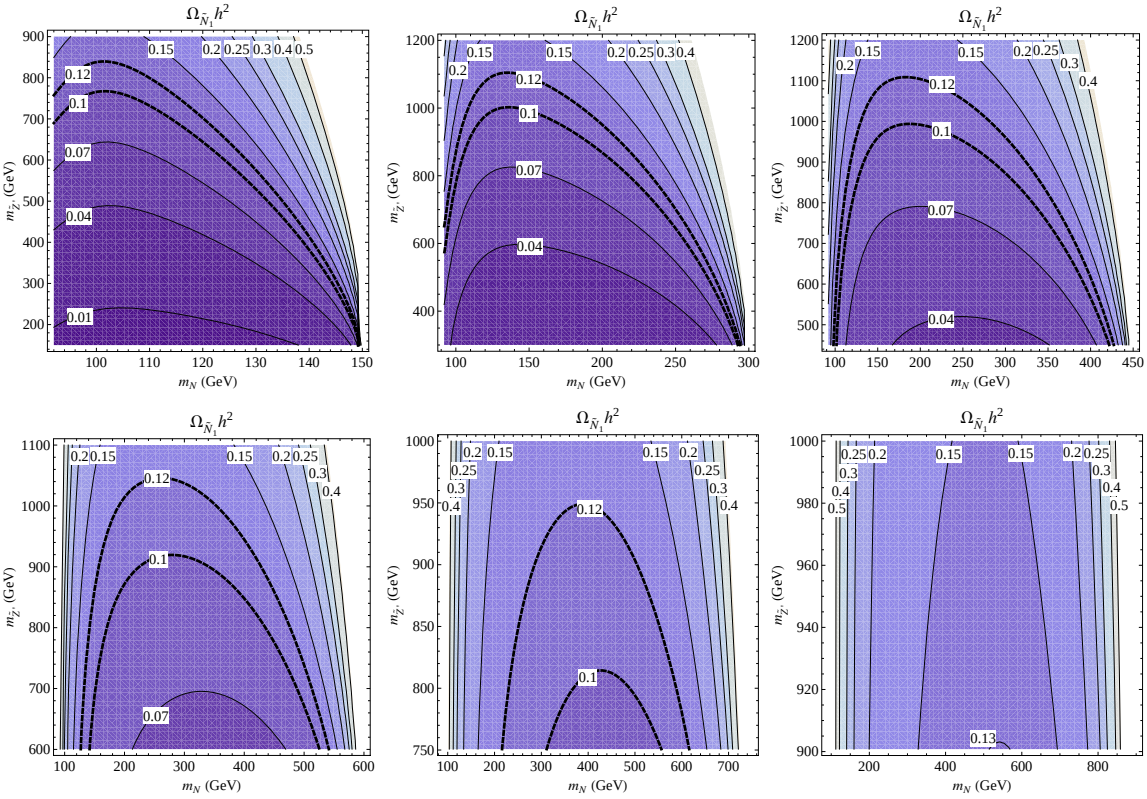

Figure 5: Contour plots for the relic abundance of the right-handed sneutrino dark matter $\widetilde{N}_1$ in the $m_N - m_{\widetilde{Z}'}$ plane. The panels show the cases $m_{\widetilde{N}_1} = 150$, 300, 450, 600, 750 and 900 GeV respectively from left to right and top to bottom. We fix the other parameters as follows: $M_{Z'} = 1200$ GeV and $\widetilde{m}_\nu = 10^{-3}$ eV. In each panel, the region between two thick dashed lines is preferred by the recent result on the DM relic density.

neutrino annihilates to the SM fermions trough the s-channel Z' mediation. In Figure 7, we therefore present the thermal relic abundance $\Omega_{\widetilde{N}_1}h^2$ in the m_N–$m_{\widetilde{Z}'}$ parameter space to check the dependence of the relic abundance $\Omega_{\widetilde{N}_1}h^2$ on the Z' mass $M_{Z'}$. In the figure, the left-panel corresponds to $M_{Z'} = 2000$ GeV and the right-panel to $M_{Z'} = 4000$ GeV. In this analysis, we use the numerical values $m_{\widetilde{N}_1} = 300$ GeV and $\widetilde{m}_\nu = 10^{-3}$ eV. The parameter space between two thick dashed lines is also the region which is allowed by the recent WMAP observational result on the DM relic density [17].

The decoupling of the right-handed sneutrino DM particle $\widetilde{N}_1$ from thermal equilibrium is determined by the $\widetilde{N}_1\widetilde{N}_1$ annihilation to right-handed neutrinos through the t-channel $\widetilde{Z}'$ exchange if the right-handed neutrino N remains in thermal equilibrium. Therefore, the relic density of the right-handed sneutrino DM barely depends on the $U(1)'$ gauge boson mass $M_{Z'}$ if the right-handed neutrino remains in thermal equilibrium by some other interactions when the DM particle $\widetilde{N}_1$ is decoupled. This is the case with large values of the effective neutrino mass, $\widetilde{m}_\nu \gtrsim 10^{-3}$ eV, for which the decays and inverse decays of the right-handed neutrino become dominant interactions before the annihilation of N freezes

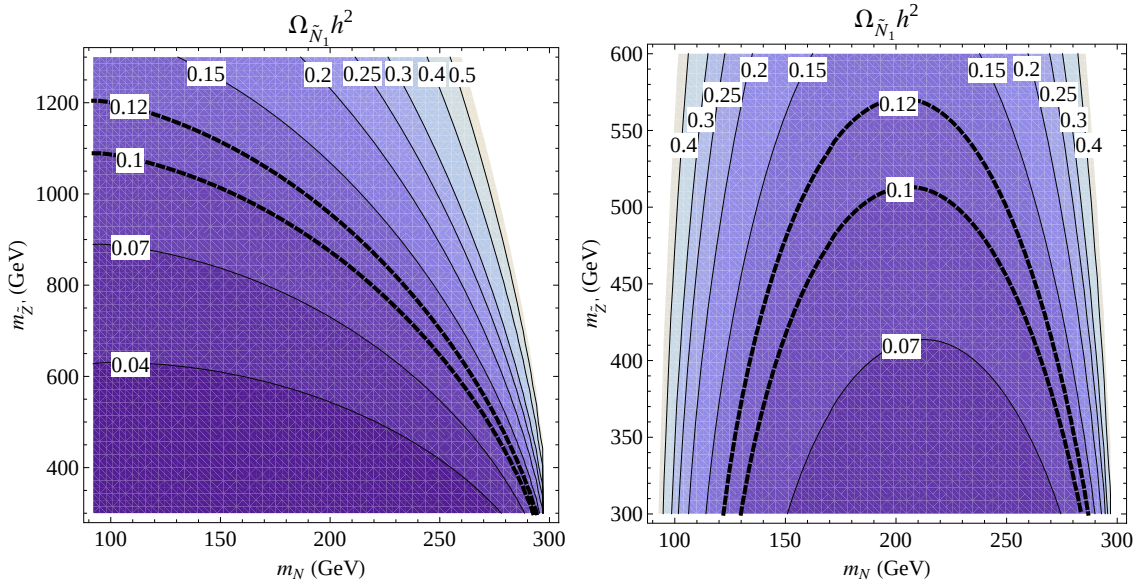

Figure 6: Contour plots for the relic abundance of right-handed sneutrino dark matter $\widetilde{N}_1$ in the $m_N - m_{\widetilde{Z}'}$ plane. Left and right panels are respectively corresponding to $\widetilde{m}_\nu = 10^{-1}$ and 10^{-5} eV. The parameters $m_{\widetilde{N}_1}$ and $m_{Z'}$ are fixed as $m_{\widetilde{N}_1} = 300$ GeV and $M_{Z'} = 1200$ GeV. In each plane, the region between two thick dashed lines is allowed by the recent DM relic density result.

out. Thus, the right-handed neutrino remains continuously in thermal equilibrium during the freeze-out of the DM $\tilde{N}_1$ as can be seen clearly from the top-left panel of Figure 4 with $\tilde{m}_\nu = 10^{-2}$ eV. Consequently, one can expect that the relic abundance of $\widetilde{N}_1$ has almost no dependence on the Z' gauge boson mass. However, for smaller values of the effective neutrino mass, $\widetilde{m}_\nu \lesssim 10^{-3}$ eV, the annihilation of N may freeze out before the decay modes of N become important, and hence the decoupling effect of the NN annihilation is non-negligible. As $M_{Z'}$ increases, the NN annihilation cross section becomes smaller, and thus the NN annihilation decouples earlier. Because of this, the relic density of the right-handed sneutrino DM becomes larger. Comparing the top-middle panel of Figure 5 and the two panels of Figure 7 with $M_{Z'} = 1.2, 2$ and 4 TeV, respectively, one can find the fact that the thermal relic abundance $\Omega_{\widetilde{N}_1}h^2$ increases as the Z' gauge boson mass increases, and thus the right dark matter density is obtained for smaller $\tilde{Z}'$ mass.

3.5 Dependence on g'

In all analysis of this paper, we use $g' = \sqrt{5/3}g_2 \tan\theta_W \approx 0.46$ as the reference value for $U(1)'$ gauge coupling [7]. However, in this section, we vary the $U(1)'$ gauge coupling to show the dependence of the relic abundance of $\widetilde{N}_1$ on this gauge coupling. In the left two panels of Figure 8, we present the thermal relic density of $\widetilde{N}_1$ for two cases $g' = 0.3$ and $g' = 0.25$ with $m_{\widetilde{N}_1} = 300$ GeV; in the right panel, for the case $g' = 0.2$ with $m_{\widetilde{N}_1} = 150$ GeV. In all the cases, we use the same numerical values for the other parameters: $M_{Z'} = 1200$ GeV and $\widetilde{m}_\nu = 10^{-3}$ eV. As in the previous cases, the regions between two thick dashed lines

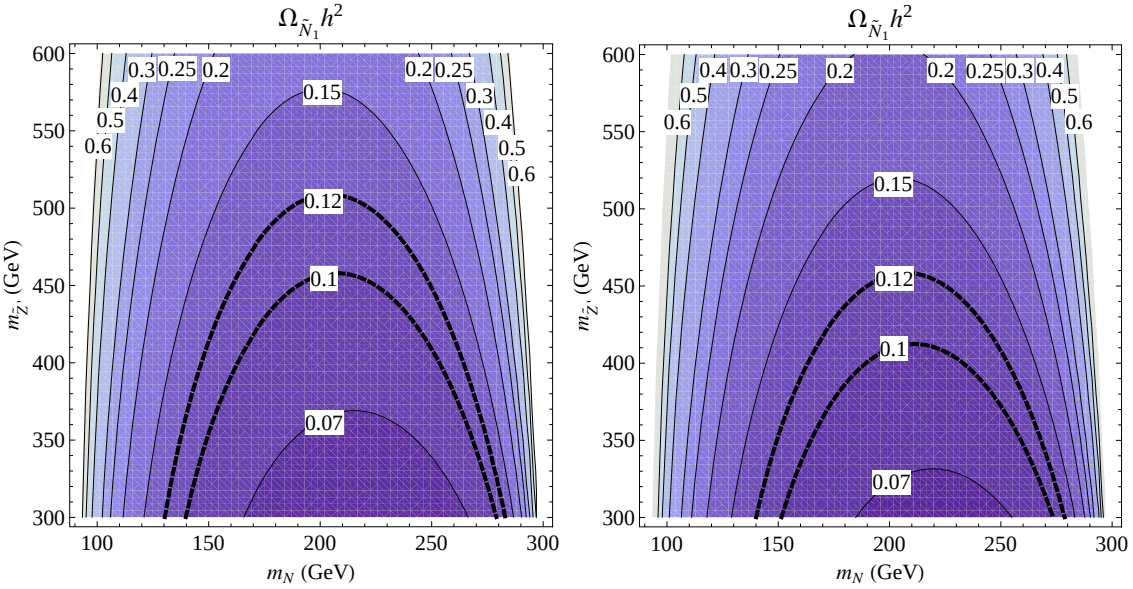

Figure 7: Contour plots for the relic abundance of the right-handed sneutrino dark matter $\widetilde{N}_1$ in the $m_N - m_{\widetilde{Z}'}$ plane for the cases $M_{Z'} = 2000$ and 4000 GeV. The parameters $m_{\widetilde{N}_1}$ and $\widetilde{m}_\nu$ are fixed as $m_{\widetilde{N}_1} = 300$ GeV and $\widetilde{m}_\nu = 10^{-3}$ eV. The regions between two thick dashed lines are preferred by the recent result on the DM relic density.

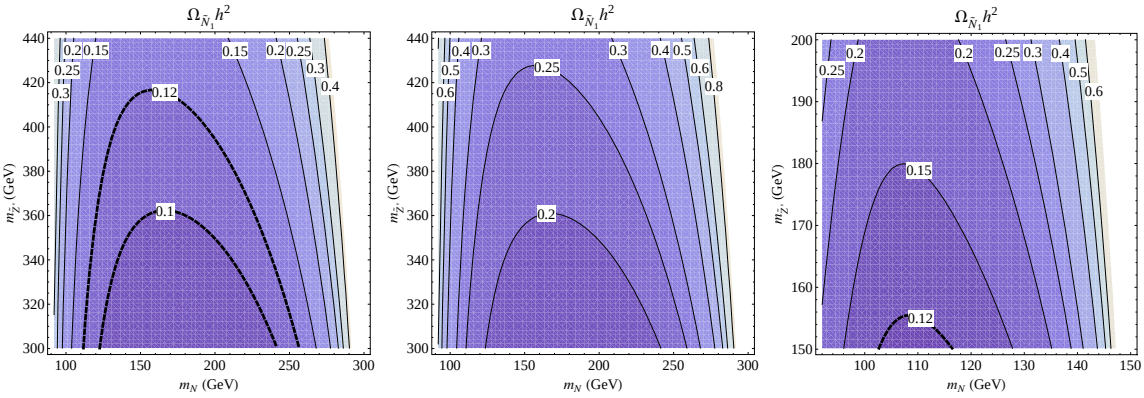

Figure 8: Contour plots for the relic abundance of the right-handed sneutrino dark matter $\widetilde{N}_1$ in the $m_N - m_{\widetilde{Z}'}$ plane. The left two panels respectively show $g' = 0.3$ and $g' = 0.25$ with $m_{\widetilde{N}_1} = 300$ GeV, and the right panel shows $g' = 0.2$ with $m_{\widetilde{N}_1} = 150$ GeV. We fix the other parameters as follows: $M_{Z'} = 1200$ GeV and $\widetilde{m}_\nu = 10^{-3}$ eV. The regions between two thick dashed lines are allowed by the recent DM relic density observation.

are consistent with the recent DM relic density observation [17].

Obviously, for smaller g', the interactions of $\widetilde{N}_1$ and N become weaker, and thus the right-handed sneutrino DM is decoupled earlier from thermal bath. Consequently, the thermal relic density of DM increases, which can be seen from the top-middle (top-left) panel of Figure 5 and the left two panels (right panel) of Figure 8. As can be seen from the

left two panels of Figure 8, the right-handed sneutrino is overproduced for $g' \lesssim 0.25$ if $\widetilde{N}_1$ is heavier than 300 GeV. When $\widetilde{N}_1$ is light enough, $m_{\widetilde{N}_1} \approx 150$ GeV, the allowed parameter space marginally exists even for $g' = 0.2$. Such a low limit is almost independent of the effective neutrino mass if $\tilde{m}_\nu \gtrsim 10^{-3}$ eV.

As a result, an interesting lower bound on the $U(1)'$ gauge coupling $g' \gtrsim 0.2$ can be put by the current dark matter relic density limit [17] in the $U(1)_\chi$ model with the right-handed sneutrino dark matter.

4. LHC signatures

For the smoking gun signal of this model, we look for the productions and decays of the new particles in the model. These include the extra gauge boson Z', its superpartner $\tilde{Z}'$, the right-handed neutrino N and the LSP dark matter $\tilde{N}_1$ being a superpartner of N. The standard search for an extra gauge boson Z' is through the observation of high mass dilepton resonances from $Z' \to l^+ l^-$ [9]. When the extra $U(1)'$ is associated with the seesaw mechanism as in this model, it is also important to look for the mode $Z' \to NN$ [10, 11, 12] to test the Majorana nature of neutrinos and the seesaw mechanism. In this section, we will discuss the associated phenomenology of $\tilde{Z}'$, which is required to be lighter than Z' as was discussed in the previous section, in parallel with the Z' phenomenology.

4.1 Production and decay of Z'

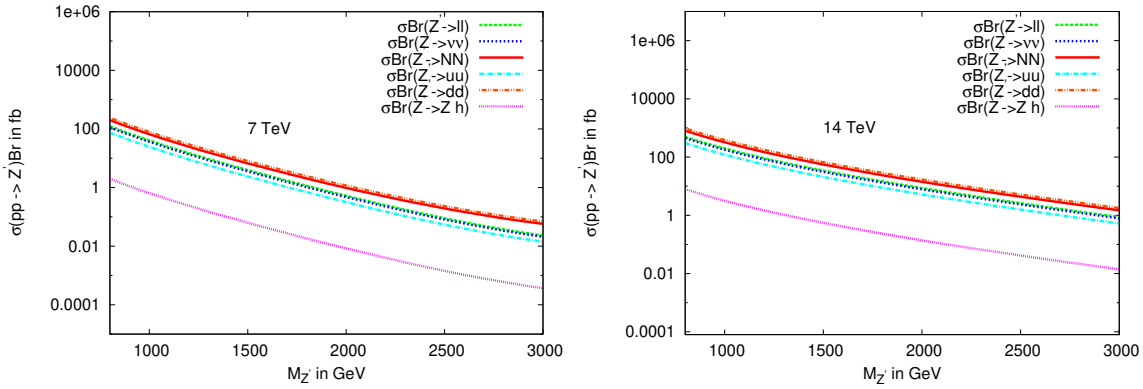

Figure 9: The Z' production cross-section times the branching ratios for the SM channels including right-handed neutrinos. Two panels are for $\sqrt{\hat{s}} = 7$ and 14 TeV, respectively, with $\tan\beta = 10$.

Single Z' produced at the LHC like the Standard Model Z can be observed through its decay modes. All the possible decay channels are shown in Table 1 for the supersymmetric $U(1)_\chi$ model. Our main focus is the production of the right-handed neutrinos through the process $pp \to Z' \to NN$ which can be compared with the standard Z' discovery channel $pp \to Z' \to l^\pm l^\mp$. In this paper, we assume that the Z' decays to sfermions are not allowed kinematically. In Figure 9, we show the production cross-section for each SM decay channel of Z' including right-handed neutrinos in the decoupling limit of non-SM Higgs

bosons. The mass of the right-handed neutrino was taken to be 300 GeV for the set of plots. The renormalization/factorization scale was chosen to be $\sqrt{\hat{s}}$ and CTEQ6L [18] was taken as PDF for the cross-section calculation. Apart from the dilepton and NN channels, the Higgs modes could also be interesting. For the quark, lepton and right-handed neutrino modes in Figure 9, we have shown only one flavor contributions. One can see that the down type quark mode has larger cross-section than the up type quark as well as the leptonic modes, which is consistent with the charges given in Eq. (2.1). By the same reason, the NN production cross-section is the largest, which enhances the Majorana neutrino signatures (see Subsection 4.3) compared to other $U(1)'$ models. Concerning the Higgs contribution, we have considered only the SM Higgs which leads to the Zh mode. This has a very low cross-section for large $\tan\beta$ as the coupling is proportional to $\cos(\alpha+\beta)$ which is $\sin(2\beta)$ in the decoupling limit. Thus, for low $\tan\beta$, the Higgs cross-section gets enhanced and comparable to the fermionic modes. Let us also remark that the production cross-section of the standard Z' discovery channel, $Z' \to l^{\pm}l^{\mp}$, depends on $\tan\beta$ and on the number of new channels, e.g., with Higgs bosons or sfermions that can be kinematically allowed in our model. In the case of a $U(1)'$ extension of the non-supersymmetric Standard Model, the model dependence comes only from the number of right-handed neutrino channels.

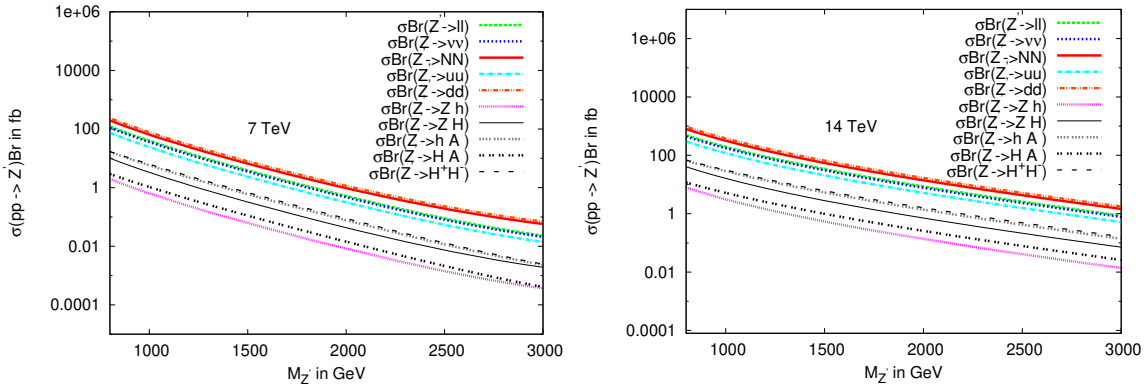

Figure 10: Same as in Figure 9 but with non-decoupling heavy Higgs bosons.

Figure 10 describes the case with all the possible Higgs decay modes, which includes Z' decays to HZ, hA, HA and $H^{\pm}H^{\mp}$. For this study, we have taken the CP-odd Higgs to be non-decoupled , i.e. $m_A = 162.2$ GeV, which makes the charged Higgs mass 180 GeV and the heavy neutral Higgs 164 GeV. As can be seen in Figure 10, the production cross-sections are not promising at least for the case of center of mass energy of 7 TeV. In the 14 TeV case, $H^{\pm}H^{\mp}$ and hA can approach the production cross-section ~ 100 fb at $\tan\beta = 10$. The other Higgs channels, HA, hZ and HZ, do not have enough effective-cross section at 14 TeV. At $\tan\beta = 10$, $\sin(\alpha+\beta) \simeq 1$, which makes the h–A–Z' and Z'–$H^{\pm}$–$H^{\mp}$ couplings almost same (see Table 1) which is also reflected in Figure 10. The ratio of the production cross-section between hA and HA is proportional to $\left(\frac{\sin(\alpha+\beta)}{\cos(\alpha+\beta)}\right)^2$ and the same is the case for ZH and Zh, as is expected from the nature of their couplings given in Table 1. It is also to be noticed that Higgs pair production channels have more production rates

compared to associated gauge boson channels due to the momentum dependent couplings of the formers. Given the suppressed Higgs channels, the production cross-sections for the NN and ll modes remain almost same as in the decoupling limit.

4.2 Production and decay of $\tilde{Z}'$

Unlike Z' whose mass is strongly constrained by the precision electroweak data, its superpartner $\tilde{Z}'$ can be light, as required in the model of the right-handed sneutrino dark matter. Thus, it can lead to interesting phenomenology related to the seesaw mechanism even though Z' turns out to be too heavy to be produced at the LHC.Let us first try to look for the direct pair production of $\tilde{Z}'$ at the LHC. In Figure 11, we estimate the pair production rate, *i.e.* $pp \to \tilde{Z}'\tilde{Z}'$, with the variation of $m_{\tilde{Z}'}$ at the LHC for the center of mass energy of 7 TeV and 14 TeV. The renormalization/factorization scale was chosen to be $\sqrt{\hat{s}}$ and CTEQ6L [18] was taken as PDF for the cross-section calculation as was in the previous case. The rates appear to be very low for both 7 and 14 TeV cases, due to the fact that only t-channel electroweak diagrams contribute to the process. This results in the production cross-section $\sim$ fb even for the light $\tilde{Z}'$.

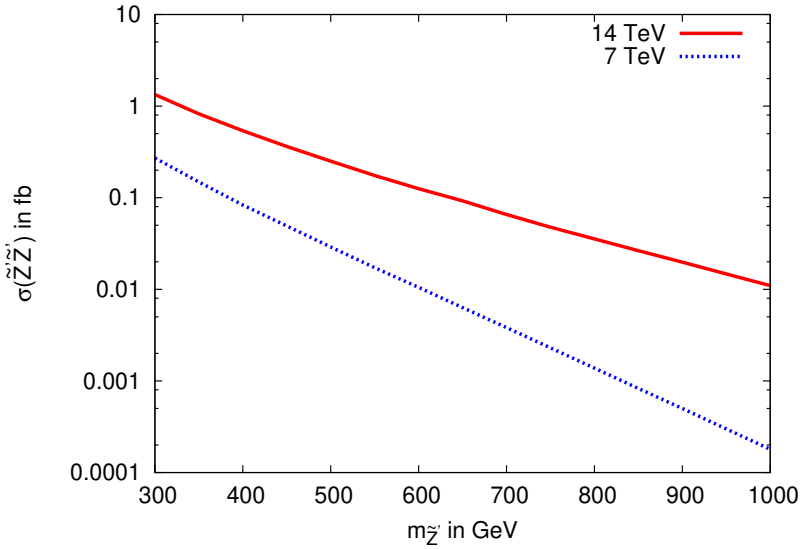

Figure 11: Variation of $\tilde{Z}'\tilde{Z}'$ production cross-section.

However, let us note that the LHC being a machine with huge gluon flux, the strongly interacting supersymmetric particles namely squarks and gluino can be copiously produced. Cascade decays of such supersymmetric colored particles could then be a good source of superpartners of the electroweak particles. In particular, squarks decay through the direct electroweak couplings to quarks and neutralinos or charginos, and gluinos decay through the two-body decay to squarks and quarks or through three-body decay to quark pair and charginos or neutralinos. An interesting application of such supersymmetric cascade decays to the Higgs production has been studied [19] in the context of MSSM.

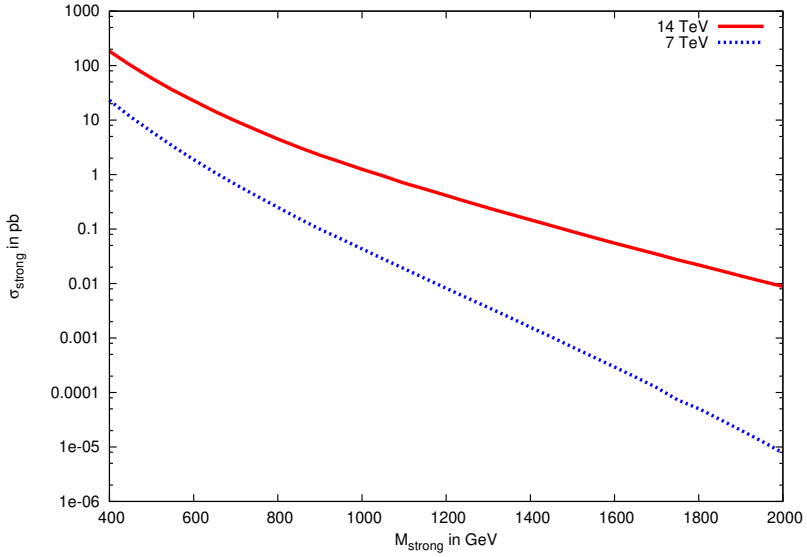

Figure 12: Variation of strong production cross-section.

Figure 12 describes the variation of strong production rate with the common mass M_{strong} of squarks and gluinos for the center of mass energy of 7 TeV and 14 TeV including the contributions from only first two generations of squarks. For $M_{\text{strong}} = 1$ TeV, the cross-sections are 43 fb and 1.3 pb for the 7 and 14 TeV center of mass energy, respectively. The inclusion of third generation will of course enhance the production rate. This can be compared to the $Z' \to NN$ production cross-sections for $M_{Z'} = 1$ TeV: 70 fb and 350 fb for the 7 and 14 TeV for one generation of right handed neutrino, respectively. Inclusion of three generation will increase the production cross-section by factor 3. The numbers of $\tilde{Z}'$ and Z' events will sensitively depend on the masses of squarks/gluinos and Z'. The squarks and gluinos can now decay to $\tilde{Z}'$. The branching fraction to $\tilde{Z}'$ depends on the mass parameters and on the coupling with left and right-handed up and down type quarks as shown in Eq. (2.1). Figure 13 describes the $\tilde{q} \to q\tilde{Z}'$ branching fraction with the variation of the squark mass for $m_{\tilde{Z}'} = 300$ GeV, 500 GeV and 700 GeV. From the figure, we can see that the $\tilde{d}_R \to d\tilde{Z}'$ has larger branching fraction compared to other quark modes as is evident from Eq. (2.1). The charge corresponding to d_R type quark is $3/2\sqrt{10}$ which is the largest among quarks. Note that the branching ratio of $\tilde{q} \to q\tilde{Z}'$ reaches about 70% unless the kinematic suppression is applied. This will lead to a sizable number of $\tilde{Z}'$ produced from the cascade decays of squarks and gluinos. In the case of $\tilde{Z}'$ being the next lightest supersymmetric particle (NLSP), all of the pair produced strong particles will end up with a pair of $\tilde{Z}'$, i.e. the effective branching fraction is 100 %.

The decay of $\tilde{Z}'$ can give rise to various final states depending on the possible decay modes that are open: that is, $\tilde{Z}' \to N\tilde{N}, l\tilde{l}, H\tilde{H}$ and $S_{1,2}\tilde{S}_{1,2}$. Here H and $\tilde{H}$ denote any type of Higgs bosons and Higgsinos shown in Table 1. The $U(1)'$ Higgs bosons, $S_{1,2}$, or Higgsinos, $\tilde{S}_{1,2}$, are expected to be as heavy as Z' and thus heavier than $\tilde{Z}'$. Assuming the Higgsinos heavier than $\tilde{Z}'$, we will concentrate on the first two decay channels in this

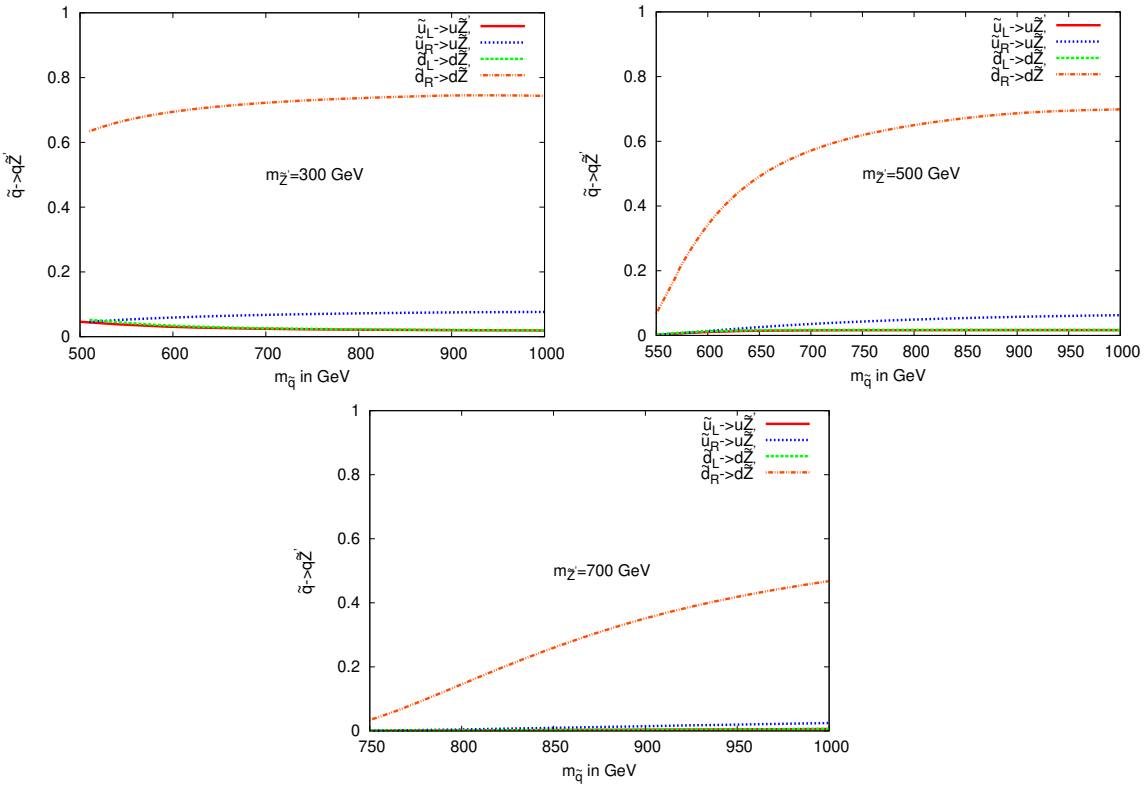

Figure 13: Variation of $\mathrm{Br}(\tilde{q} \to q\tilde{Z}')$ with M_{strong} for $m_{\tilde{Z}'} = 300$, 500, and 700 GeV respectively.

paper. Note again that the $\tilde{Z}' \to N\tilde{N}$ mode is the dominant mode given the $U(1)_\chi$ charge assignment (2.1) and becomes the unique one if $\tilde{Z}'$ is the NLSP and $\tilde{N}$ is the LSP, $\tilde{N}_1$. In the next subsection, we will focus on the mode $\tilde{Z}' \to N\tilde{N}_1$.

4.3 Signatures of the seesaw and displaced Higgses

As discussed in the previous subsections, the extra $U(1)_\chi$ gauge boson Z' and its superpartner $\tilde{Z}'$ can be copiously produced and decay to right-handed neutrinos at the LHC. Thus, we can search for the signatures of the pair produced heavy Majorana neutrinos through two channels:

$$\begin{aligned} pp &\to Z' \to NN\,, \\ pp &\to \tilde{Z}'\tilde{Z}' \to NN\tilde{N}_1\tilde{N}_1\,. \end{aligned} \tag{4.1}$$

Now, the right-handed neutrino, N, can decay to the following final states:

$$N \to lW, \nu Z, \nu h, \nu H, \nu A, lH^+ \tag{4.2}$$

as shown in Subsection 2.2.

Figure 14 describes the mass variation of the decay branching fraction of the right-handed neutrino and the partial decay widths for various decay modes for the effective

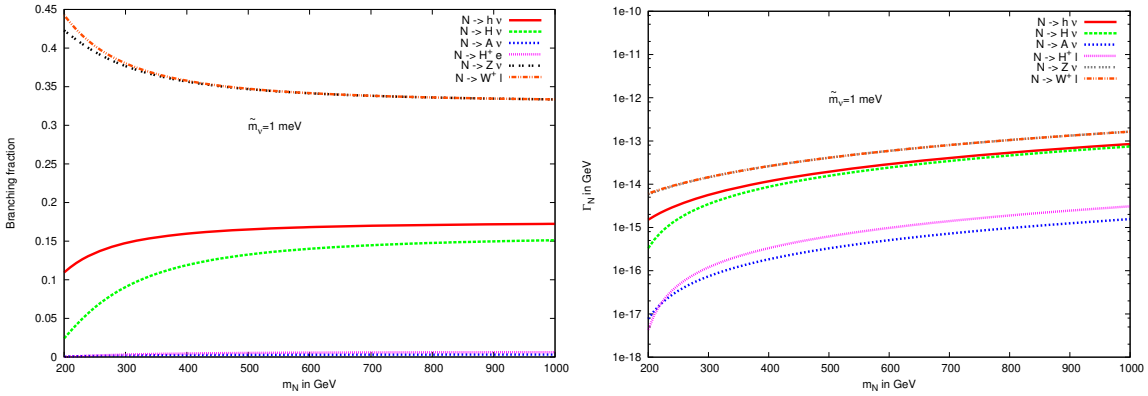

Figure 14: Branching fractions and partial decay widths of the right-handed neutrino, N, in the non-decoupling limit of heavy Higgs bosons with $m_A = 162.2$ GeV as a function of m_N for the effective neutrino mass, $\tilde{m}_\nu = 1$ meV and $\tan\beta = 10$.

neutrino mass $\tilde{m}_\nu = 1$ meV. From Figure 14, it is clear that the right-handed neutrino decays to gauge bosons and lepton modes have more decay branching fraction $\sim 35 - 45\%$ for the whole region of the right-handed neutrino mass, m_N. Apart from the production of the gauge bosons from the decay of the right-handed neutrino, Higgs modes are also possible due to the direct coupling in the superpotential Eq. (2.2) which is proportional to the small Yukawa coupling, y_ν. The mode $N \to h\nu$ has larger branching fraction compared to the $N \to H\nu$ mode, which is also expected from Eq. (2.18). The right-handed neutrino decays to the pseudo-scalar Higgs mode, i.e. $N \to A\nu$, and also the charged Higgs modes, i.e $N \to H^\pm l^\mp$, have very low branching fraction because of the fact that the decay widths are proportional to $\cos^2\beta \approx 10^{-2}$. For the choice of smaller $\tan\beta$, these modes also could be interesting.

In the model under discussion, the Majorana nature of right-handed neutrino, N, can be probed either of the two channels (4.1) leading to the same-sign dilepton (SSD) final states:

$$pp \to Z' \, (\tilde{Z}'\tilde{Z}') \to l^\pm l^\pm W^\mp W^\mp \, (+ \not{p}_T) \, . \tag{4.3}$$

Depending on the decay of $W^\pm$, the final state can have $3l$ or $4l$, or SSD + 4j $(+ \not{p}_T)$. The missing energy contribution comes from $\tilde{Z}'$ decaying to the LSP, $\tilde{N}_1$.

It is also interesting to look for the Higgs signal from the channel $N \to h\nu$. When the Yukawa coupling, y_ν, or the effective neutrino mass, $\tilde{m}_\nu$, is small enough, the Higgs thus produced will be displaced and its main decay to $b\bar{b}$ can be observed [13]. If the other right-handed neutrino, N, decays to $l^\mp W^\pm$ or νZ, then the final states can have one or two charged leptons to tag along with the $b\bar{b}$:

$$pp \to Z' \, , \; \tilde{Z}'\tilde{Z}' \to h \, l^\pm W^\mp / Z + \not{p}_T \, . \tag{4.4}$$

To get some reference values for the production cross-section of this signal, let us take $Br(N \to l^\pm W^\mp) \times Br(N \to h\nu) \approx 5\%$ from Figure 14 and there is a combinatorial factor 2 as one of the N has to decay to Higgs which makes $Br(NN \to h\nu l^\pm W^\mp) \sim$

10%. At the 7 TeV LHC, we have $\sigma(pp \to Z' \to NN) \simeq 0.07$ pb for $M_{Z'} = 1$ TeV, and $\sigma(pp \to \tilde{Z}'\tilde{Z}' \to NN) = 43$ fb for $M_{strong} = 1$ TeV assuming the $\tilde{Z}'$ NLSP as was discussed in the previous subsections. This leads to the production cross-section of the process (4.4): $\sigma(hl^{\pm}W^{\mp}) = 21$ fb and 4.3 fb from the Z' and $\tilde{Z}'$ channel, respectively. Thus, there is a chance to find the Higgs signal at the 7 TeV LHC if, in particular, the associated displaced vertex is large enough to kill the backgrounds. The corresponding figures at the 14 TeV LHC are $\sigma(hl^{\pm}W^{\mp}) = 105$ fb and 130 fb from the Z' and $\tilde{Z}'$ channels, respectively.

Figure 15 describes the variation of the decay length of right-handed neutrino, N, with the right-handed neutrino mass, m_N, for two effective masses $\tilde{m}_\nu = 1$ and 0.01 meV. One can see that the decay length becomes favorably large for $\tilde{m}_\nu \lesssim 1$ meV making clean the N decay signals. There is a large parameter space for such a effective neutrino mass allowing the right-handed sneutrino dark matter as shown in Figure 5.

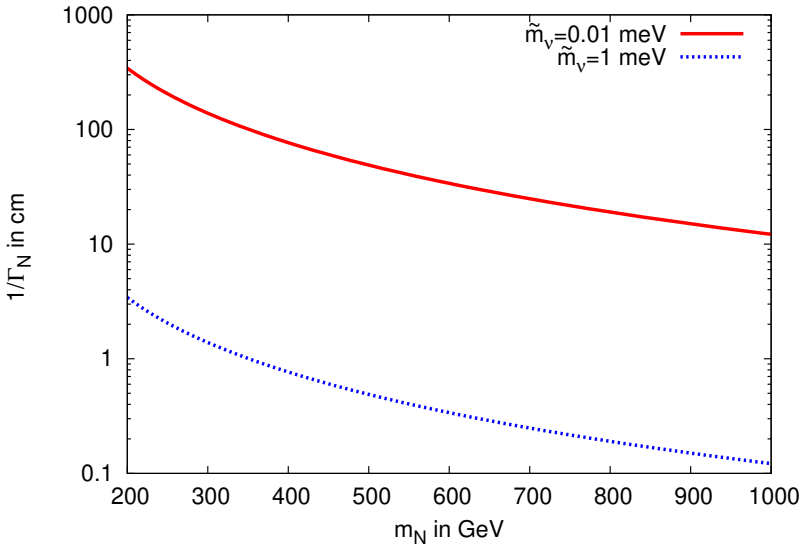

Figure 15: Variation of the decay length of the right handed neutrino for $\tilde{m}_\nu = 1$ and 0.01 meV, respectively.

For small $\tan\beta$, the right-handed neutrino, N, can have a large branching fraction to the charged Higgs and charged lepton, if kinematically allowed. Thus, we can have SSD plus charged Higgs in the final state:

$$pp \to Z' \ (\tilde{Z}'\tilde{Z}') \to H^{\pm}W^{\pm}l^{\mp}l^{\mp} \ (+ \not{p}_T) \tag{4.5}$$

in which the charged Higgs decays to $\tau\bar{\nu}_\tau$ or $t\bar{b}$. These lead to the displaced multi-jet (τ-jet or b-jet) and multi-lepton final states.

When $\tilde{Z}'$ is not the NLSP, $\tilde{Z}'$ can also contribute to $l\tilde{l}^*$ if kinematically allowed. In this situation, we can have the following final states:

$$pp \to \tilde{Z}'\tilde{Z}' \to \begin{cases} W^{\pm}l^{\mp}l^{\pm}l^{\mp} + \not{p}_T \\ Z^0 l^{\pm}l^{\mp} + \not{p}_T \\ hl^{\pm}l^{\mp} + \not{p}_T \\ H^{\pm}l^{\mp}l^{\pm}l^{\mp} + \not{p}_T \end{cases}, \tag{4.6}$$

which may involve one displaced and one prompt vertex.

The final states discussed above can be studied as smoking gun signals for this model at the LHC. Among those channels, the channels associated with the multi-lepton final states suppress the SM backgrounds effectively [20]. Again the displaced decay of the right-handed neutrino actually can remove the SM background completely. Nevertheless, still for the estimation of signal significance, one needs to consider the following backgrounds: $t\bar{t}$, $t\bar{t}Z$, $t\bar{t}h$, $W + n-$jets, and $Z + n-$jets as well as other supersymmetric final states. The detailed simulation for the above mentioned final states and the corresponding significance calculation deserve further investigation [21]. There is another aspect of this model that could be interesting through the mixing in the neutrino (2.15) and sneutrino (2.17) sector.Specially, in the context of the NLSP decaying to the LSP ($\tilde{N}_1$), these can lead to remarkable features in the final state depending on the nature of the NLSP [21].

5. Conclusion

We considered the possibility of a right-handed sneutrino as the LSP dark matter in the supersymmetric Standard Model extended to include an extra $U(1)'$ gauge symmetry realizing the seesaw mechanism with three right-handed neutrinos. In a supersymmetric seesaw model, a complex right-handed sneutrino gets split into two real mass eigenstates due to the soft supersymmetry breaking Majorana mass term. While the lightest real right-handed sneutrino, $\tilde{N}_1$ as the LSP, cannot annihilate through the $U(1)'$ gauge boson Z' exchange at the s-channel, its annihilation to lighter right-handed neutrinos, $\tilde{N}_1\tilde{N}_1 \to NN$, mediated by the $U(1)'$ gaugino $\tilde{Z}'$ at the t-channel is shown to be effective in generating the right dark matter relic density. In this process, the decay and inverse decay of N play an important role in maintaining N and $\tilde{N}_1$ longer in thermal equilibrium and thus reducing the dark matter density. This behavior was shown in Figure 4 by solving the Boltzmann equations with varying the decay rate quantified by the effective neutrino mass, $\tilde{m}_\nu$. The resulting dark matter density is computed in Figures 5, 6, 7, 8 showing the favorable parameter space of the model.

The signatures of the model can be probed through the production of Z' as well as $\tilde{Z}'$ and the corresponding decays. In particular, the production of the right-handed neutrino is of great interest because of its Majorana nature and possible displaced vertices. When $\tilde{Z}'$ is light enough as is needed for the right-handed sneutrino dark matter, it can be pair-produced copiously through the cascade decays of squarks/gluinos as estimated in Figures 12, 13 leading to a large number of events for the process of $pp \to \tilde{Z}'\tilde{Z}' \to NN + \not{p}_T$. This can be compared with the production cross-section of the usual process $pp \to Z' \to NN$ as shown in Figures 9, 10 including all the other final states except the sfermions. The above channels provide the golden search for the seesaw mechanism and the Majorana nature of neutrinos through the same-sign dilepton final states. We also point out a remarkable feature of the Higgs production from the right-handed neutrino decay. The displaced $b\bar{b}$ along with displaced tagged leptons will be a clean signature in probing the light neutral Higgs. The non-decoupled heavy Higgs bosons can also be probed in a similar way. In this article, we have given the number of the production rates and the effective branching

fractions which gives a hint that these signal topologies can be probed with early data of the LHC for the 7 TeV case. The detailed collider simulation to calculate the acceptance under the basics and the hard cuts will be reported in a separate work [21].

Acknowledgments: EJC was supported by Korea Neutrino Research Center through National Research Foundation of Korea Grant (2009-0083526).

References

[1] For a review, see, G. Jungman, M. Kamionkowski and K. Griest, Phys. Rept. **267** (1996) 195 [arXiv:hep-ph/9506380].

[2] For a review, see, R. N. Mohapatra *et al.*, Rept. Prog. Phys. **70** (2007) 1757 [arXiv:hep-ph/0510213].

[3] T. Asaka, K. Ishiwata and T. Moroi, Phys. Rev. D **73** (2006) 051301 [arXiv:hep-ph/0512118]; S. Gopalakrishna, A. de Gouvea and W. Porod, JCAP **0605**, 005 (2006) [arXiv:hep-ph/0602027].

[4] N. Arkani-Hamed, L. J. Hall, H. Murayama, D. Tucker-Smith and N. Weiner, Phys. Rev. D **64** (2001) 115011 [arXiv:hep-ph/0006312]; F. Borzumati and Y. Nomura, Phys. Rev. D **64** (2001) 053005 [arXiv:hep-ph/0007018]; G. Belanger, M. Kakizaki, E. K. Park, S. Kraml and A. Pukhov, JCAP **1011** (2010) 017 [arXiv:1008.0580 [hep-ph]].

[5] F. Deppisch and A. Pilaftsis, JHEP **0810** (2008) 080 [arXiv:0808.0490 [hep-ph]]; D. G. Cerdeno and O. Seto, JCAP **0908** (2009) 032 [arXiv:0903.4677 [hep-ph]].

[6] C. Arina, F. Bazzocchi, N. Fornengo, J. C. Romao and J. W. F. Valle, Phys. Rev. Lett. **101** (2008) 161802 [arXiv:0806.3225 [hep-ph]]; S. Khalil, H. Okada and T. Toma, arXiv:1102.4249 [hep-ph].

[7] P. Langacker, Rev. Mod. Phys. **81** (2009) 1199 [arXiv:0801.1345 [hep-ph]].

[8] H. S. Lee, K. T. Matchev and S. Nasri, Phys. Rev. D **76** (2007) 041302 [arXiv:hep-ph/0702223].

[9] T. Aaltonen *et al.* [The CDF Collaboration], Phys. Rev. Lett. **106**, 121801 (2011) [arXiv:1101.4578 [hep-ex]]; S. Chatrchyan *et al.* [CMS Collaboration], arXiv:1103.0981 [hep-ex]; G. Aad *et al.* [ATLAS Collaboration], arXiv:1103.6218 [hep-ex].

[10] W. Y. Keung and G. Senjanovic, Phys. Rev. Lett. **50** (1983) 1427.

[11] P. Langacker, R. W. Robinett and J. L. Rosner, Phys. Rev. D **30** (1984) 1470.

[12] For some LHC studies, see, A. Ferrari *et al.*, Phys. Rev. D **62** (2000) 013001; F. del Aguila and J. A. Aguilar-Saavedra, JHEP **0711** (2007) 072 [arXiv:0705.4117 [hep-ph]]; K. Huitu, S. Khalil, H. Okada and S. K. Rai, Phys. Rev. Lett. **101** (2008) 181802 [arXiv:0803.2799 [hep-ph]]; L. Basso, A. Belyaev, S. Moretti and C. H. Shepherd-Themistocleous, Phys. Rev. D **80** (2009) 055030 [arXiv:0812.4313 [hep-ph]]; P. F. Perez, S. Spinner and M. K. Trenkel, arXiv:1103.5504 [hep-ph].

[13] P. Bandyopadhyay and E. J. Chun, JHEP **1011** (2010) 006 [arXiv:1007.2281 [hep-ph]].

[14] S. Khalil and A. Masiero, Phys. Lett. B **665** (2008) 374 [arXiv:0710.3525 [hep-ph]].

[15] U. Ellwanger, C. Hugonie and A. M. Teixeira, Phys. Rept. **496** (2010) 1 [arXiv:0910.1785 [hep-ph]].

[16] J. Erler, P. Langacker, S. Munir and E. R. Pena, JHEP **0908**, 017 (2009) [arXiv:0906.2435 [hep-ph]].

[17] E. Komatsu *et al.* [WMAP Collaboration], Astrophys. J. Suppl. **192**, 18 (2011) [arXiv:1001.4538 [astro-ph.CO]].

[18] J. Pumplin, D. R. Stump, J. Huston, H. L. Lai, P. M. Nadolsky and W. K. Tung, JHEP **0207** (2002) 012 [arXiv:hep-ph/0201195].

[19] A. Datta, A. Djouadi, M. Guchait and Y. Mambrini, "Charged Higgs production from SUSY particle cascade decays at the CERN [arXiv:hep-ph/0107271]. A. Datta, A. Djouadi, M. Guchait and F. Moortgat, "Detection of mssm higgs bosons from supersymmetric particle cascade decays Nucl. Phys. B **681**, 31 (2004) [arXiv:hep-ph/0303095]. P. Bandyopadhyay, A. Datta and B. Mukhopadhyaya, Phys. Lett. B **670** (2008) 5 [arXiv:0806.2367 [hep-ph]]. P. Bandyopadhyay, JHEP **0907** (2009) 102 [arXiv:0811.2537 [hep-ph]]. P. Bandyopadhyay, arXiv:1008.3339 [hep-ph].

[20] F. del Aguila and J. A. Aguilar-Saavedra, Nucl. Phys. B **813** (2009) 22 [arXiv:0808.2468 [hep-ph]].

[21] P. Bandyopadhyay, E. J. Chun and J. C. Park, work in progress.